Supplementary Material for

Thermodynamic and Kinetic Analysis of an RNA Kissing Interaction and Its Resolution into an Extended Duplex

Nilshad Salim[*], Rajan Lamichhane[*], Rui Zhao, Tuhina Banerjee, Jane Philip, David Rueda[‡] and Andrew L Feig[‡]

Prof. Andrew L. Feig or
Prof. David Rueda
Department of Chemistry
Wayne State University
5101 Cass Ave.
Detroit, MI 48202
Phone: 313-577-9229
Fax: 313-577-8822
Email: afeig@chem.wayne.edu or david.rueda@wayne.edu

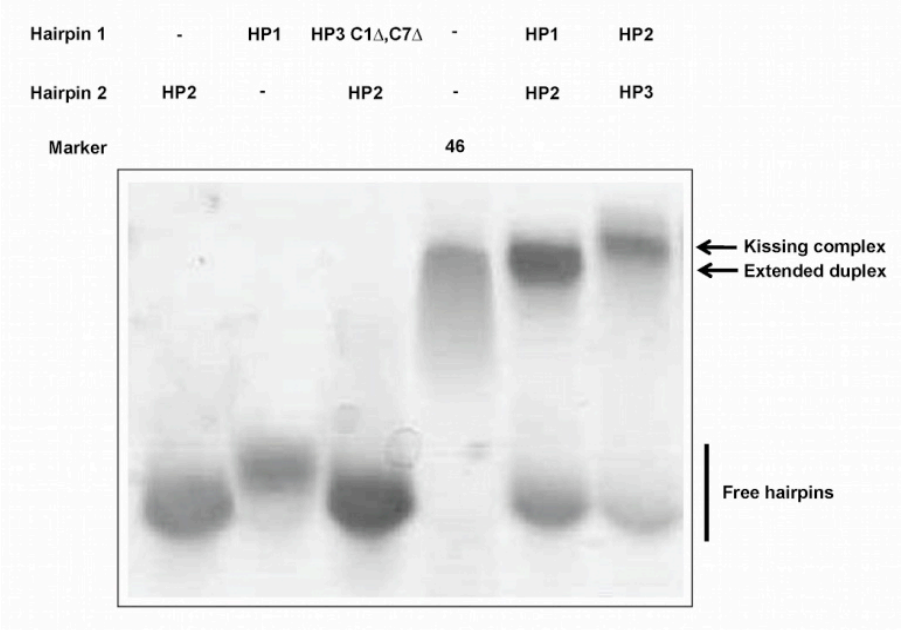

Figure S1. Native gel analysis of kissing and extended duplex formation. Lanes 1 and 2 consist of hairpins HP2 and HP1. In lane 3, the interaction between HP3-C1Δ,C7Δ::HP2 is probed. Lane 5 and 6 probes for extended duplex formation between HP1 and HP2 and the kissing complex between HP1 and HP3. Lane 4 comprises a 46 size marker.

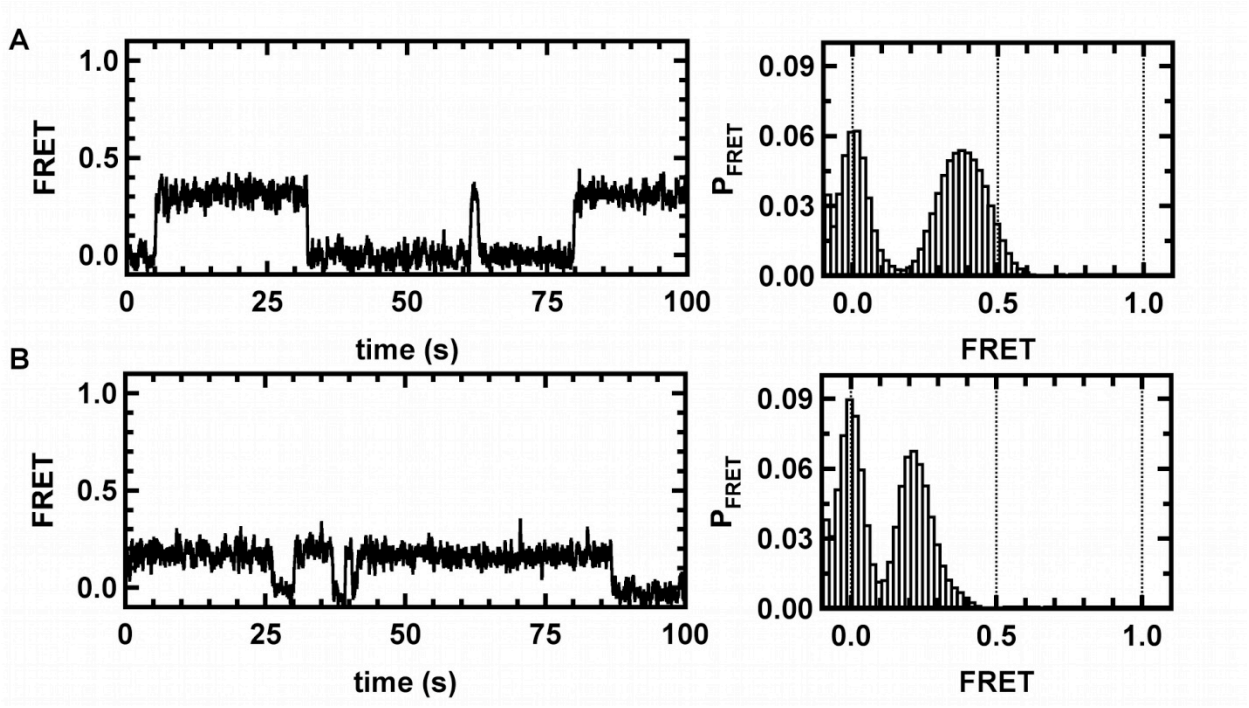

Figure S2. (A) Representative single time trajectory and FRET histogram of HP1 forming kissing complex with HP2-Stem2 (HP2-Stem2; 5' AUA ACA GAA CAG GGG AAA UGC CUG UUC UGU, has a longer stem region than parent HP1 with four additional base pairs). (B) Representative single time trajectory and FRET histogram of HP1-Stem2 (HP1-Stem2; 5' ACG GAA CAG GCA UUU CCC CUG UUC UGU) forming kissing complex with HP2-Stem2.

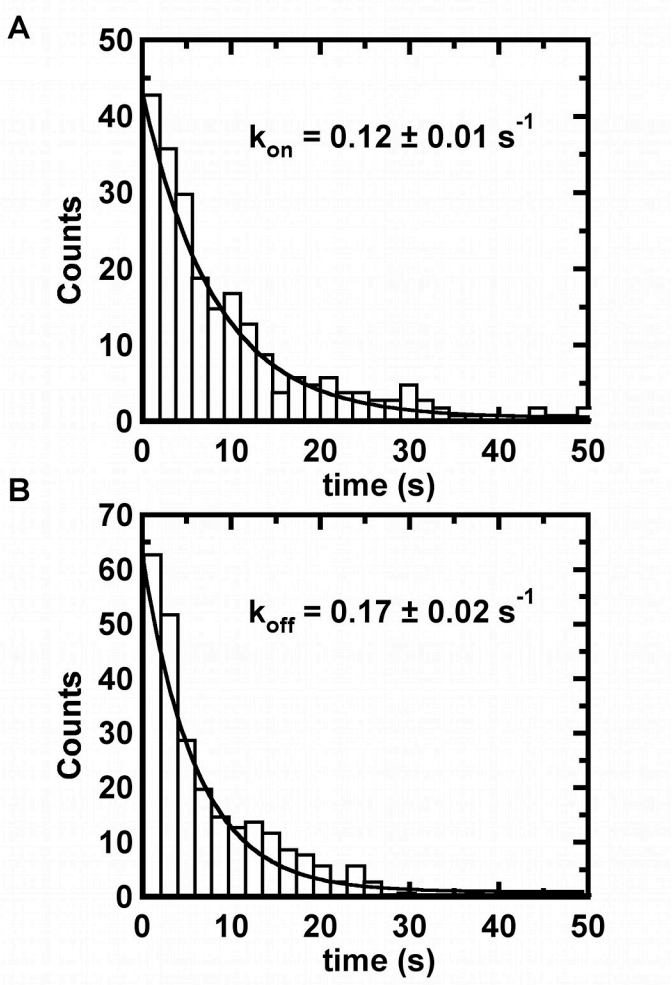

Figure S3. Dwell time distributions for single-molecule trajectories. Association (A) and dissociation (B) of HP1::HP2 kissing complexes. Each distribution was fit to a single-exponential decay to yield the pseudo-first order rate constants k_{on} and k_{off}.

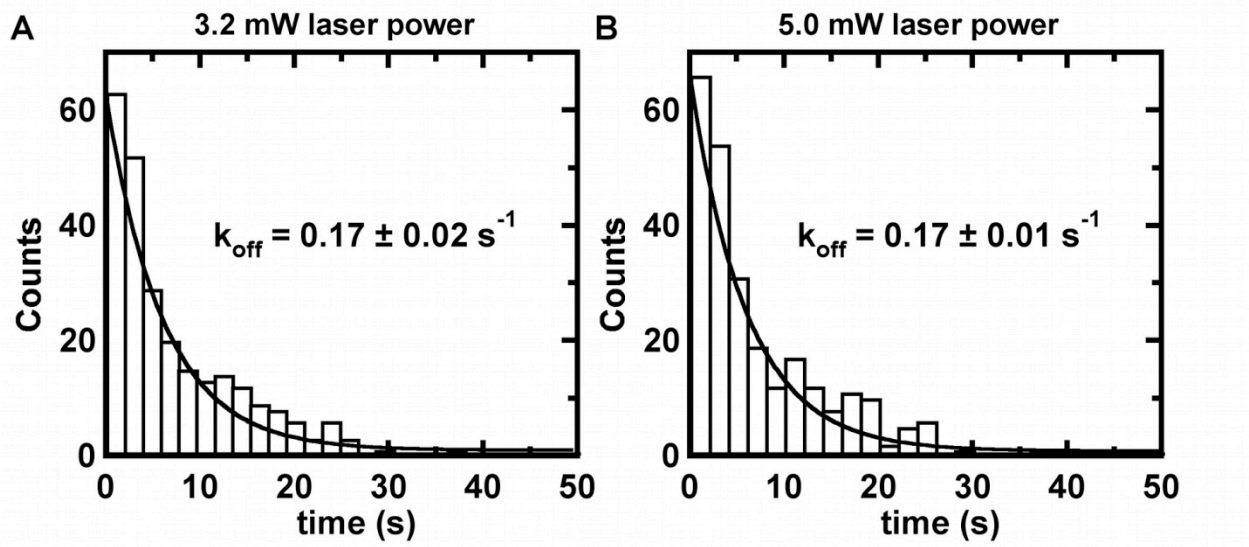

Figure S4. Kissing complex dissociation reaction rate at laser irradiation power of 3.2 mW (A) and 5.0 mW (B).

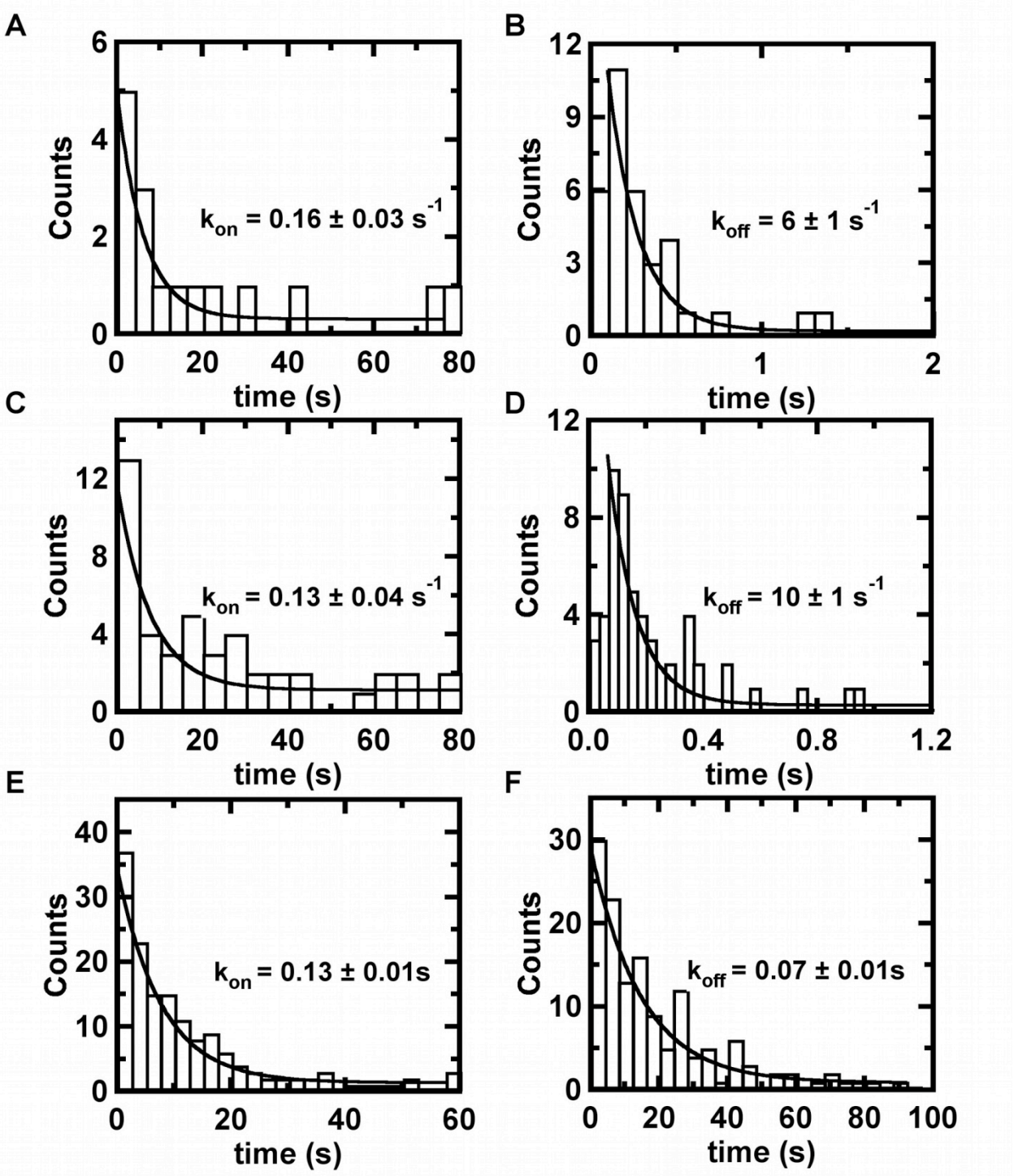

Figure S5. (A) Apparent kissing complex formation rate for HP1-C7A with 35 nM of HP2. (B) Kissing complex dissociation reaction rate for HP1-C7A with 35 nM of HP2. (C) Apparent kissing complex formation rate for HP1-C1A with 35 nM of HP2. (D) Kissing complex dissociation reaction rate for HP1-C1A with 35 nM of HP2. (E) Apparent kissing complex formation rate for HP1-U4G with 35 nM of HP2-A4C. (F) Kissing complex dissociation reaction rate for HP1-U4G with 35 nM of HP2-A4C.

Table S1. Summary of thermodynamic parameters obtained from UV melting experiments

Construct	1 M NaCl		10 mM $MgCl_2$	
	T_M (°C)	ΔH^{UV} (ΔH)[a] (kcal/mol)	T_M (°C)	ΔH^{UV} (ΔH)[a] (kcal/mol)
Hairpins				
HP3	60.6	-47	62.5	-57
HP1-C1A	63.9	-51	76.2	-64
HP1	60.8	-49	66.3	-38
HP2	71.5	-41	76.1	-42
HP2-A(3-5)C	72.1	-28	81.9	-47
HP1-U4G	61.7	-55	67.8	-47
HP2-A4C	71.2	71	76	51
Duplexes				
HP1::HP2	84.7	-110	84.3	-154
HP1::HP2-A(3-5)C	74.6	-52	67.8	-43

[a] The estimated error for ΔH^{UV} (ΔH) for all individual data points is ± 1 kcal/mol and T_M is ± 0.4°C, based on replicate measurements.

Table S2. Thermodynamic parameters obtained by ITC for the kissing interaction of HP1::HP3 and HP2-A4C::HP3-U4G in 10 mM NaHEPES, pH 7.5. N.B. – no binding; n.d. – not determined

System	Ionic Condition	T (˚C)	ΔH kcal/mol	ΔS cal/mol•K	ΔG kcal/mol	K_a x 10^6 (M^{-1})	n
Kissing complex (HP2::HP3)	1 M NaCl	10	-41.2 ± 0.1	-116 ± 10	-8.4 ± 0.9	2.8 ± 0.3	0.9
		25	-25.9 ± 0.2	-58 ± 10	-9 ± 1	1.7 ± 0.3	0.9
		35	-21.7 ± 0.2	-43 ± 10	-9 ± 2	1.1 ± 0.2	0.9
		45	N.B.	-	-	-	-
	10 mM $MgCl_2$	10	-14.9 ± 0.3	-19 ± 10	-10 ± 1	38 ± 1	0.9
		25	-29.9 ± 0.7	-69 ± 10	-9 ± 2	8 ± 1	0.9
		35	n.d.	-	-	-	-
		45	-29.9 ± 0.2	-67 ± 10	-9 ± 1	1.0 ± 0.1	0.9
Kissing Complex (HP2-4C)::(HP3-4G)	1 M NaCl	10	-26 ± 1	-56 ± 9	-9.8 ± 0.1	37 ± 1	0.9
		15	-28 ± 3	-64 ± 12	-9.9 ± 0.1	37 ± 6	0.9
		20	-39 ± 1	-99 ± 8	-10.3 ± 0.9	130 ± 90	0.8
		30	-35 ± 8	-79 ± 26	-10.7 ± 0.5	690 ± 40	0.9
		40	-23 ± 1	-38 ± 10	-10.7 ± 0.5	31 ± 4	1.0
	10 mM $MgCl_2$	15	-34.4 ± 1	-83 ± 9	-10.5 ± 0.5	90 ± 1	0.9
		20	-39.4 ± 1	-99 ± 10	-10.4 ± 0.5	55 ± 1	0.9
		25	-39.7 ± 1	-98 ± 8	-10.5 ± 0.5	50 ± 9	0.8
		30	-46.0 ± 1	-119 ± 13	-10.2 ± 0.5	23 ± 4	0.9
		40	-37.6 ± 1	-86 ± 10	-10.5 ± 0.5	51 ± 2	1.0

Table S3. Thermodynamic parameters measured using ITC in 1M NaCl for RNA duplexes with sequences associated with kissing hairpins

System	Temperature ° C	ΔH (kcal/mol)	ΔS (cal/mol K)	ΔG (kcal/mol)
	5	-39 ± 1	-108 ± 3	-9.6 ± 0.8
	10	-39 ± 3	-104 ± 11	-9.5 ± 0.1
	15	-43 ± 2	-117 ± 6	-9.1 ± 0.1
	15	-37 ± 4	-93 ± 12	-10.4 ± 0.2
	20	-50 ± 6	-136 ± 18	-10.3 ± 0.4
	25	-61 ± 1	-171 ± 1	-10.2 ± 0.1
	5	-15 ± 3	-27 ± 10	-8.1 ± 0.5
	10	No binding in ITC		
	15			
		No binding in ITC		

Table S4. Comparison between stabilities predicted by nearest neighbor parameters (NN) and experimentally measured values for RNA duplex and kissing complex formation (27, 36, 37).

System	Context	ΔG^{NN} kcal/mol	ΔG^{Exp} kcal/mol	$\Delta\Delta G^{Exp-NN}$ kcal/mol	$\Delta\Delta G^{Exp(kissing)-NN (duplex)}$ kcal/mol
RNA2:RNA3	Duplex	-6.7	-6.8	0.1	
HP2::HP3	Kissing	N/A	-8.3	N/A	-1.6
RNA2-A4C:RNA3-U4G	Duplex	-9.2	-8.0	1.2	
HP2-A4C::HP3-U4G	Kissing	N/A	-11.2	N/A	-2

Table S5. Thermodynamic parameters obtained for strand displacement reaction of HP1::HP2 and HP1::HP2-A(3-5)C to form the extended duplex in 10 mM Na HEPES, pH 7.5.

Interaction	Ionic Condition	T ˚C	ΔH (kcal/mol)	ΔS[a] (cal/mol K)	ΔG (kcal/mol)	K_a x 10^6 (M^{-1})	n
HP1::HP2	1 M NaCl	15	-37.3 ± 0.9	-99	-8.8 ± 0.9	3.8 ± 0.4	1.0
		25	-52.3 ± 0.3	-146	-9 ± 1	2.6 ± 0.3	0.9
		35	-62.3 ± 0.2	-171	-9.6 ± 0.6	7.7 ± 0.5	1.0
		45	-75.9 ± 0.2	-208	-10 ± 1	4.3 ± 0.5	1.0
	10 mM $MgCl_2$	15	-32.7 ± 0.6	-80	-10 ± 1	17 ± 2	1.0
		25	-52.8 ± 0.2	-147	-9 ± 2	3.8 ± 0.7	0.8
		35	-76 ± 1	-214	-9.8 ± 0.4	8.1 ± 0.3	0.9
		45	-84 ± 1	-234	-10 ± 1	5.7 ± 0.8	0.9
HP1::HP2-A(3-5)C	1 M NaCl	25	-34.2 ± 0.6	-86	-9 ± 1	1.9 ± 0.2	0.9
		45	-70.4 ± 0.3	-192	-9 ± 1	2.7 ± 0.5	0.9

[a] The estimated error for ΔS is ±10 cal $mol^{-1}K^{-1}$, based on replicate measurements.

Table S6. Kinetic parameters measured using surface plasmon resonance (SPR) and smFRET for kissing complex formation in 10 mM $MgCl_2$. From kinetic measurements obtained using SPR, ΔG was calculated. Activation energies were computed using the temperature dependence of the kinetics according to the Eyring's equation (Materials and Methods). $k_{a,\ app}$: Apparent association rate constants for kissing interactions measured using smFRET, where the pseudo-first order rate was divided by the effective ligand concentration of 35 nM.

		SPR									*smFRET*			
					Association			Dissociation						
System	T (°C)	k_a x 10^{-4} ($M^{-1}s^{-1}$)	k_d x 10^{-4} (s^{-1})	ΔG (kcal/mol)	$\Delta G^{\ddagger}_{298}$ (kcal/mol)	$\Delta H^{\ddagger}$ (kcal/mol)	$\Delta S^{\ddagger}$ (cal/mol K)	$\Delta G^{\ddagger}_{298}$ (kcal/mol)	$\Delta H^{\ddagger}$ (kcal/mol)	$\Delta S^{\ddagger}$ (cal/mol K)	$k_{a,\ app}$ x 10^{-5} (s^{-1})	k_d (s^{-1})	ΔG_{298} (kcal/mol)	$\Delta\Delta G_{298}$ (kcal/mol)
HP2/HP3	10	1.3 ± 0.1	2.3 ± 0.2	-10.0 ± 0.1										
	15	1.5 ± 0.2	3.0 ± 0.2	-10.2 ± 0.1										
	25	1.9 ± 0.1	15 ± 1	-9.7 ± 0.1	11 ± 1	5 ± 1	-24 ± 1	21 ± 1	26 ± 1	16 ± 1	3.4 ± 0.3	0.18 ± 0.02	-9.9 ± 0.2	-
	30	3.8 ± 0.2	38 ± 2	-9.7 ± 0.1										
	40	3.1 ± 0.5	180 ± 20	-9.0 ± 0.1										
HP2-A4C/HP3-U4G	10	2.2 ± 0.2	2.30 ± 0.08	-10.3 ± 0.1										
	15	3.0 ± 0.3	1.2 ± 0.4	-11.0 ± 0.2										
	25	3.6 ± 0.8	0.9 ± 0.2	-11.7 ± 0.2	11 ± 1	4 ± 1	-24 ± 1	23 ± 2	32 ± 4	33 ± 5	3.7 ± 0.3	0.07 ± 0.01	-10.5 ± 0.2	-0.6 ± 0.3
	30	4.7 ± 0.2	3.0 ± 0.3	-11.3 ± 0.1										
	35	3.4 ± 0.1	8.2 ± 0.4	-10.7 ± 0.1										
HP1-C1A/HP2	25										4.7 ± 0.9	6 ± 1	-8.0 ± 0.2	1.9 ± 0.3
HP1-C7A/HP2	25										4 ± 1	10 ± 1	-7.6 ± 0.3	2.3 ± 0.4

Materials and Methods

RNA constructs used

Figure 1B summarizes the RNA hairpins used in this study. Nucleotide sequences (loop nucleotides are underlined) are: HP1 has the sequence 5′-GGACGAGGCAUUUCCCCUUGU-3′. HP3 has a RNA sequence of 5′-GGACGAUCAGCAUUUCCCUGAUGU-3′, HP3-C1A,C7A 5′-GGACGAUCAGAAUUUCACUGAUGU-3′, HP3-C1A 5'- GGACGAUCAGAAUUU CCCUGA UGU-3′, HP3-C7A 5'-GGACGAUCAGCAUUUCACUGAUGU-3′, HP3-C1Δ,C7Δ 5′-GGACGAUCAGAUUUCCUGAUGU-3′, HP3-U4G 5'- GGACGAUCAGCAUGUCCCUGAUGU-3′. HP2 5′-GGACAAGGGGAAAUGCCUUGU-3′ and the HP2-A(3-5)C is 5′-GGACAAGGGGCCCGGCCUUGU-3′, HP2-A3C 5'- GGACAAGGGGCAAUGCCUUGU-3', HP2-A4C 5'-GGACAAGGGGACAUGCCUUGU-3'. RNA oligomers were synthesized by Dharmacon/Thermo Scientific (Lafayette, CO). RNAs were deprotected using the procedures specified by the manufacturer and were purified by denaturing PAGE, eluted into 0.5 M ammonium acetate, ethanol precipitated, and resuspended in water. Concentrations of RNA stock solutions were determined by absorbance at 260 nm (49).

UV melting studies

Absorbance versus temperature profiles (melting curves) were measured with an Aviv 14DS UV-VIS spectrophotometer with a five-cuvette thermoelectric controller as previously described (55). Custom-manufactured microcuvettes (Hellma Cells) with 0.1 cm and 0.2 cm path lengths (60 and 120μL volumes, respectively) were used. Oligonucleotides were dissolved in 10 mM NaHEPES, pH 7.5 containing either 1.0 M NaCl or 10 mM $MgCl_2$. Samples were annealed and degassed by raising the temperature to 85 °C for 5 min and then cooling to -1.6 °C over a period of 25 min just prior to a melting experiment. Care was taken not to allow the total absorbance to rise above 2.0. While at 85 °C, the absorbance was measured at 260 nm for later calculation of oligonucleotide concentration using the extinction coefficients. Thermodynamic parameters for hairpin and duplex formation were derived from the thermal melting data using the program MELTWIN v.3.0 (51). This program uses the Marquardt-Levenberg non-linear least squares method to solve for ΔH and ΔS and upper and lower baselines from absorbance versus temperature profiles. The above method assumes a two-state model and a $\Delta C_P = 0$ for the transition equilibrium. Thus, these parameters are most accurate at the melting temperature of the system.

Isothermal Titration Calorimetry (ITC)

A VP-ITC titration calorimeter (MicroCal, Inc.) was used for all measurements. Samples were prepared by diluting a small volume of stock into 10 mM NaHEPES, pH 7.5 and 1.0 M added NaCl. The syringe and sample cell RNAs were prepared in matched buffers to minimize background heats of dilution. All buffers were prepared from stock solutions on the day of use and extensively degassed under vacuum. Samples were heated at 95 °C for 3 min and cooled at room temperature for 30 min prior to data collection. After an initial 2 μL injection to counteract backlash in the auto-titrator (52), ITC experiment consisted of 40 injections (at 7 μL per injection) of a 60 μM

oligonucleotide into 1.4 mL of the complementary strand at 3.5 μM. Sample stirring was set at 310 rpm for all measurements. Titration data were collected at several different temperatures. ITC data were analyzed with ORIGIN software (MicroCal Inc., ver. 7.0). Raw thermograms were integrated and normalized, resulting in a plot of ΔH (mol of injectant)$^{-1}$ versus molar ratio. In each experiment, a long upper baseline was collected after the binding transition was saturated. The terminal 10 points (i.e., the clearly linear portion) of the upper baseline in each experiment were fit to a straight line, which was subsequently subtracted from the entire data set to remove contributions from background heats of mixing and dilution. A total ΔH for each reaction was obtained by nonlinear least-squares fitting of the plot of ΔH (mol of injectant)$^{-1}$ versus molar ratio to a single site binding model (56) to obtain ΔH, K_A, and the reaction stoichiometry, n under each condition. ΔG was obtained from K_A and ΔS was subsequently derived based on the Gibbs equation at each temperature and errors were estimated based on standard propagation.

Temperature dependence of ΔH was quite significant for both kissing complex formation as well as conversion of the hairpins to extended duplexes, indicating a non-zero heat capacity change (ΔC_P) for these transitions (28, 29). The reaction enthalpy was plotted as a function of temperature to obtain ΔC_P based on eq. 1 using the approximation that ΔC_P is temperature independent (28). Deviations from linearity begin to occur about 15-20 °C below the melting temperature of the product (kissing hairpin or extended duplex depending on the experiment) due to incomplete formation of reaction products at equilibrium. Only the linear portion of the data was used to compute ΔC_P.

$$\Delta C_P = d(\Delta H) / dT \qquad (1)$$

Native polyacrylamide gel electrophoresis

Complex formations between pairs of hairpins were verified using native gel electrophoresis on 20% polyacrylamide gels. Samples were prepared in 50 mM Tris-acetate buffer pH 7.5 containing 10 mM $MgCl_2$. After allowing them to equilibrate, 2 μL of 40% (wt/vol) sucrose was added and the RNA was loaded immediately onto the native gels while applying a potential of 300 V. Species were resolved under constant power (5 W for 6 – 12 hrs) at 4 °C. The running buffer for these gels was 50 mM Tris-acetate at pH 7.5 containing 10 mM $MgCl_2$. Bands were visualized by staining with StainsAll.

Surface Plasmon resonance

Kinetic experiments were performed on a Biacore 2000 instrument. Experiments were done on a streptavidin-coated chip (SA chip, Biacore). All experiments were performed in the same reaction buffer (50 mM Tris-HCl, pH 7.5, 10 mM $MgCl_2$). During all experiments ~15 fmol of 5' biotin labeled RNAs were immobilized on the sensor chip. Immobilizations of RNAs were performed at a flow rate of 5 μL/min to make sure homogeneous surface coverage is attained. Experiments were carried out at temperatures from 10 – 40 °C and at flow rates of 30 - 50 μL/min. Change in flow rates did not affect the rate constants observed in the experiments implying the absence of mass transfer effects in the conditions used.

To measure kinetics of kissing complex formation, varying concentrations of hairpins (400 – 800) nM were titrated into the surface immobilized complimentary hairpin. At the end of each injection (1 min injection) the dissociation was observed in the presence of binding buffer. Surface regeneration was performed by injecting 300 µL of regeneration buffer (50 mM Tris-HCl pH 7.5, 20 mM EDTA) at a flow rate of 100 µL/min. The data were analyzed globally by fitting both the dissociation and association (where applicable) phases simultaneously (BIA evaluation software version 4.1) using a 1:1 (Langmuir) model (two fitting parameters). BIA evaluation uses Marquardt-Lavenberg algorithm to optimize parameters in fits and assigns kinetic constants to the binding models. The goodness of the fit was judged by the reduced chi-square (χ^2) values.

RNA biotinylation

HP3 and HP3-U4G were 5'-labled with biotin to be used in surface plasmon resonance experiments. RNAs were first treated with Calf Intestinal Phosphatase (CIP) and phosphorylated using ATP-γ-S using the Ambion Kinase Max kit (Ambion, Inc). In brief, 1 nmol of RNA was treated with CIP (in 10X dephosphorylation buffer, 0.5 units of CIP at 37 °C for 2 h). The reaction mixture was purified using the Phosphatase Removal Reagent as described in the product manual. Purified RNAs were phosphorylated with ATP-γ-S using T4 Polynucleotide kinase. Phosphorylated RNAs were purified using a G-25 spin column (GE Healthcare) and speed vacuumed to dryness. RNAs were then dissolved in 45 µL of 100 mM $KHPO_4$, pH 8.0, 5 µL of 20 mM N-iodoacetyl-N-biotinylhexylenediamine dissolved in DMF (EZ-Link Iodoacetyl-LC-Biotin, Thermo Scientific). The reaction was incubated at 45 °C for 1 h while shaking under dark conditions. The reaction was then ethanol precipitated and analyzed using PAGE.

Calculation of activation energetics

The temperature dependence of k_a and k_d was analyzed according to the Eyring's equation shown below.

$$\ln\frac{k}{T} = -\frac{\Delta H^{\ddagger}}{RT} + \ln\frac{k_B}{h} + \frac{\Delta S^{\ddagger}}{R} \qquad (2)$$

In a plot of ln (k/T) vs.1/T (Figure 3B), activation enthalpy ($\Delta H^{\ddagger}$) derives from the slope and activation entropy ($\Delta S^{\ddagger}$) is obtained from the intercept. The activation energy ($\Delta G^{\ddagger}_{298}$) was calculated by using the Van't Hoff relationship.

Single-Molecule Förster Resonance Energy Transfer (smFRET)

To characterize the dynamic behavior of the kissing complex and its progression through the strand displacement reaction, smFRET was used. HP-2 and its derivatives were labeled with a 3'-Cy3 (FRET donor) and a 5'-biotin for surface immobilization on microscope slides, as described previously (53). HP1 and its derivatives were labeled with a 5'-Cy5 (FRET acceptor). The two unpaired guanosines at the 5' end of the hairpin constructs were removed in the smFRET experiments to avoid fluorophore stacking and quenching (50). Labeled hairpins were purified by gel electrophoresis and C-8 reverse phase HPLC chromatography as described previously (54). The hairpins were designed

to exhibit low FRET in the dissociated state, intermediate FRET in the kissing complex and high FRET in the duplex form. The single-molecule experiments were carried out in large excess (35 nM) of the acceptor hairpin such that the association step can be assumed to follow pseudo-first-order reaction kinetics, which greatly simplifies the data analysis and allows dissection of the reaction mechanism.

The fluorophore-labeled biotinylated donor (HP2) was surface-immobilized at low concentrations (10 pM) onto a streptavidin-BSA coated quartz slide surface via the biotin-streptavidin interaction, and excited at 532 nm in a total internal reflection fluorescence microscope. The anti-correlated donor (I_D) and acceptor (I_A) fluorescence signals from optically-resolved single molecules were detected using a back illuminated electron multiplied CCD camera (Andor). Single-step photobleaching confirmed single-molecule detection. The FRET ratio, defined as $I_A/ (I_A + I_D)$, was followed in real time for each molecule. All solutions contained 50 mM Tris-HCl and 10 mM $MgCl_2$ at pH 7.5, with an oxygen scavenging system consisting of 10% (wt/vol) glucose, 2% (vol/vol) 2-mercaptoethanol, 50 μg/mL glucose oxidase, and 10 μg/mL catalase to reduce photobleaching. All experiments were performed at room temperature.

Supplementary References

27. Freier, S. M., R. Kierzek, M. H. Caruthers, T. Neilson, and D. H. Turner. 1986. Free energy contributions of G.U and other terminal mismatches to helix stability. Biochemistry 25:3209-3213.

28. Mikulecky, P. J., and A. L. Feig. 2006. Heat capacity changes associated with nucleic acid folding. Biopolymers 82:38-58.

29. Mikulecky, P. J., and A. L. Feig. 2006. Heat capacity changes associated with DNA duplex formation: salt- and sequence-dependent effects. Biochemistry 45:604-616.

36. SantaLucia, J., Jr. 2007. Physical principles and visual-OMP software for optimal PCR design. Methods Mol Biol 402:3-34.

37. Xia, T., J. SantaLucia, Jr., M. E. Burkard, R. Kierzek, S. J. Schroeder, X. Jiao, C. Cox, and D. H. Turner. 1998. Thermodynamic parameters for an expanded nearest-neighbor model for formation of RNA duplexes with Watson-Crick base pairs. Biochemistry 37:14719-14735.

49. Fasman, G. D. 1976. CRC Handbook of Biochemistry and Molecular Biology. CRC Press LLC, Boca Raton, FL.

50. Iqbal, A., S. Arslan, B. Okumus, T. J. Wilson, G. Giraud, D. G. Norman, T. Ha, and D. M. Lilley. 2008. Orientation dependence in fluorescent energy transfer between Cy3 and Cy5 terminally attached to double-stranded nucleic acids. Proc Natl Acad Sci U S A 105:11176-11181.

51. McDowell, J. A., and D. H. Turner. 1996. Investigation of the structural basis for thermodynamic stabilities of tandem GU mismatches: Solution structure of

r(GAGGUCUC)2 by 2-D NMR and simulated annealing. Biochemistry 35:14077-14089.

52. Mizoue, L. S., and J. Tellinghuisen. 2004. The role of backlash in the "first injection anomaly" in isothermal titration calorimetry. Anal Biochem 326:125-127.

53. Rueda, D., G. Bokinsky, M. M. Rhodes, M. J. Rust, X. Zhuang, and N. G. Walter. 2004. Single-molecule enzymology of RNA: essential functional groups impact catalysis from a distance. Proc Natl Acad Sci U S A 101:10066-10071.

54. Rueda, D., and N. G. Walter. 2006. Fluorescent energy transfer readout of an aptazyme-based biosensor. Methods Mol Biol 335:289-310.

55. SantaLucia, J., Jr. 2000. The use of spectroscopic techniques in the study of DNA stability. In Spectrophotometry and Spectrofluorimetry. M. Gore, editor. University Press, Oxford, NY. 329-354.

56. Wiseman, T., S. Williston, J. Brandts, and L. Lin. 1989. Rapid measurement of binding constants and heats of binding using a new titration calorimeter. Anal Biochem 179:131-135.